Supplementary Information

Resolving Atomistic Structure and Oxygen Evolution Activity in Nickel Antimonates

Karun K. Rao,[1,2] Lan Zhou,[3,4] Yungchieh Lai,[3,4] Matthias H. Richter,[3,4] Xiang Li,[5,6] Yubing Lu,[7] Junko Yano,[6,7] John M. Gregoire,[3,4,*] Michal Bajdich[1,**]

[1] SUNCAT Center for Interface Science and Catalysis and Liquid Sunlight Alliance, SLAC National Accelerator Laboratory, Menlo Park, CA, USA

[2] Department of Chemical Engineering, Stanford University, Stanford, CA, USA

[3] Division of Engineering and Applied Science, California Institute of Technology, Pasadena, CA, USA

[4] Liquid Sunlight Alliance, California Institute of Technology, Pasadena, CA 91125, USA

[5] SLAC National Accelerator Laboratory, Menlo Park, CA 94025, USA

[6] Liquid Sunlight Alliance, Lawrence Berkeley National Laboratory, Berkeley, CA 94720, USA

[7] Molecular Biophysics and Integrated Bioimaging Division, Lawrence Berkeley National Laboratory, Berkeley, CA 94720, USA

*E-mail (Exp.): gregoire@caltech.edu (J.M.G.) **E-mail (Theory): bajdich@slac.stanford.edu (M.B.)

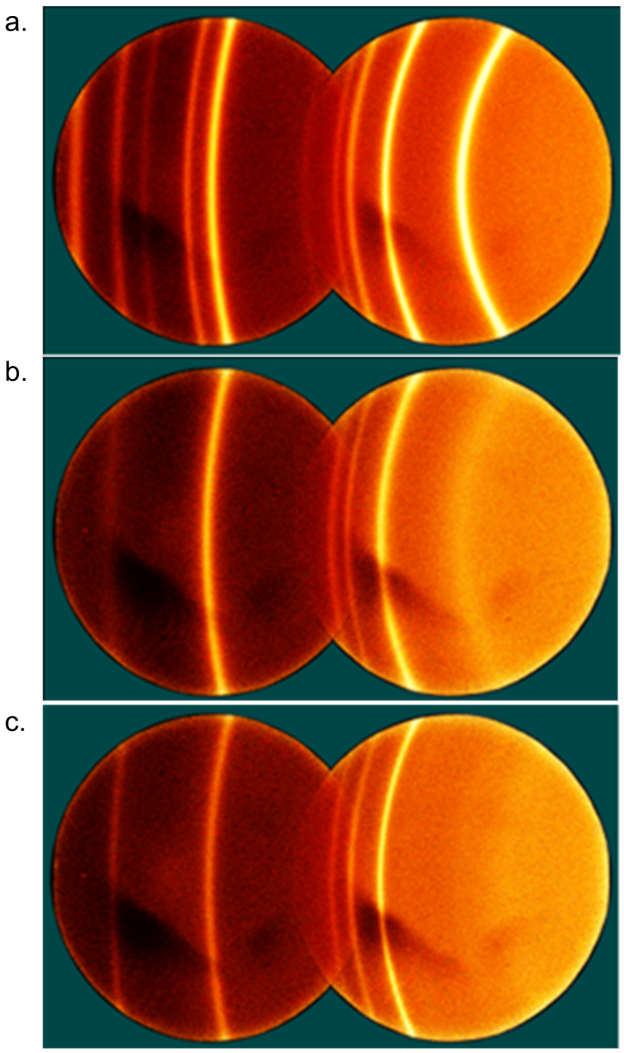

Figure S1. The raw XRD images of $Ni_xSb_{1-x}O_z$ samples (on SiO_2/Si substrate, annealed at 700 °C in air) with a) x = 0.33, b) 0.50, and c) 0.63 from Figure 1a and 1b. The diffraction rings with uniform intensity indicate an equi-axed, powder-like crystallite distribution within the thin film samples.

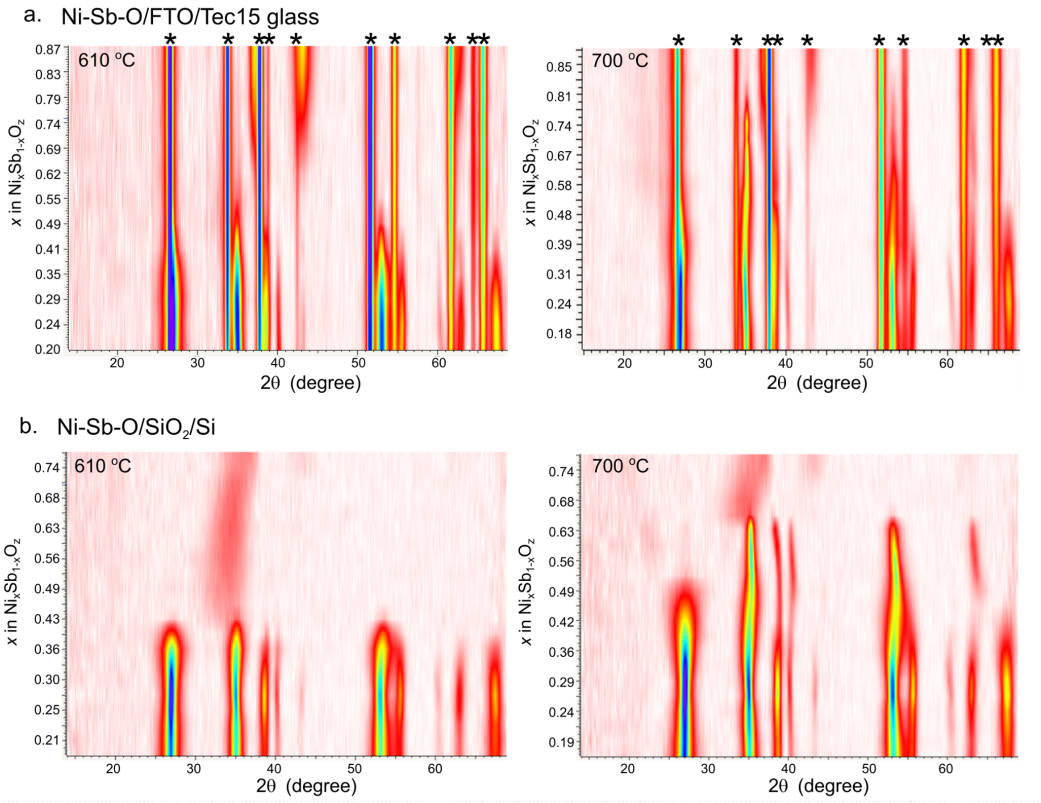

Figure S2. Heatmaps of XRD patterns for $Ni_xSb_{1-x}O_z$ composition libraries deposited on a) FTO glass and b) SiO2/Si substrates for both 610 and 700 °C post-deposition annealing temperature. Each heatmap is composed of a series of XRD patterns along the composition gradient and each data row corresponds to a 1D XRD pattern at that composition. The FTO substrate contributes to the peaks that are observed at all compositions and was indicated by * symbols.

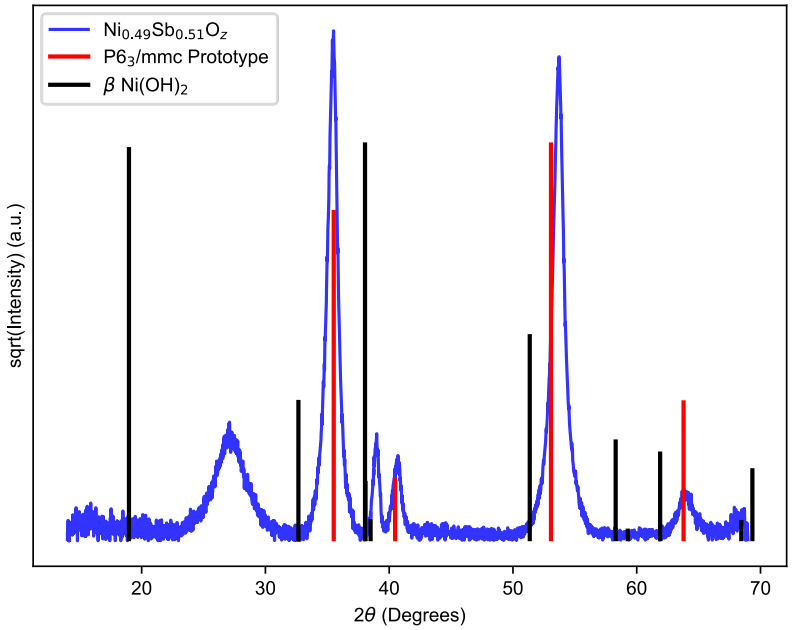

Figure S3: 1D XRD plot of the x = 0.49 composition. Black stick lines show calculated XRD pattern of β-$Ni(OH)_2$ without fitting lattice parameters. Red stick line is calculated XRD peaks of the $P6_3/mmc$ prototype with lattice constants fitted to the experimental data. The $P6_3/mmc$ prototype has the same oxygen sublattice as β-$Ni(OH)_2$, and additional metal cation sites. The β-$Ni(OH)_2$ (001) peak occurs at 19°, and is not observed in the $P6_3/mmc$ prototype.

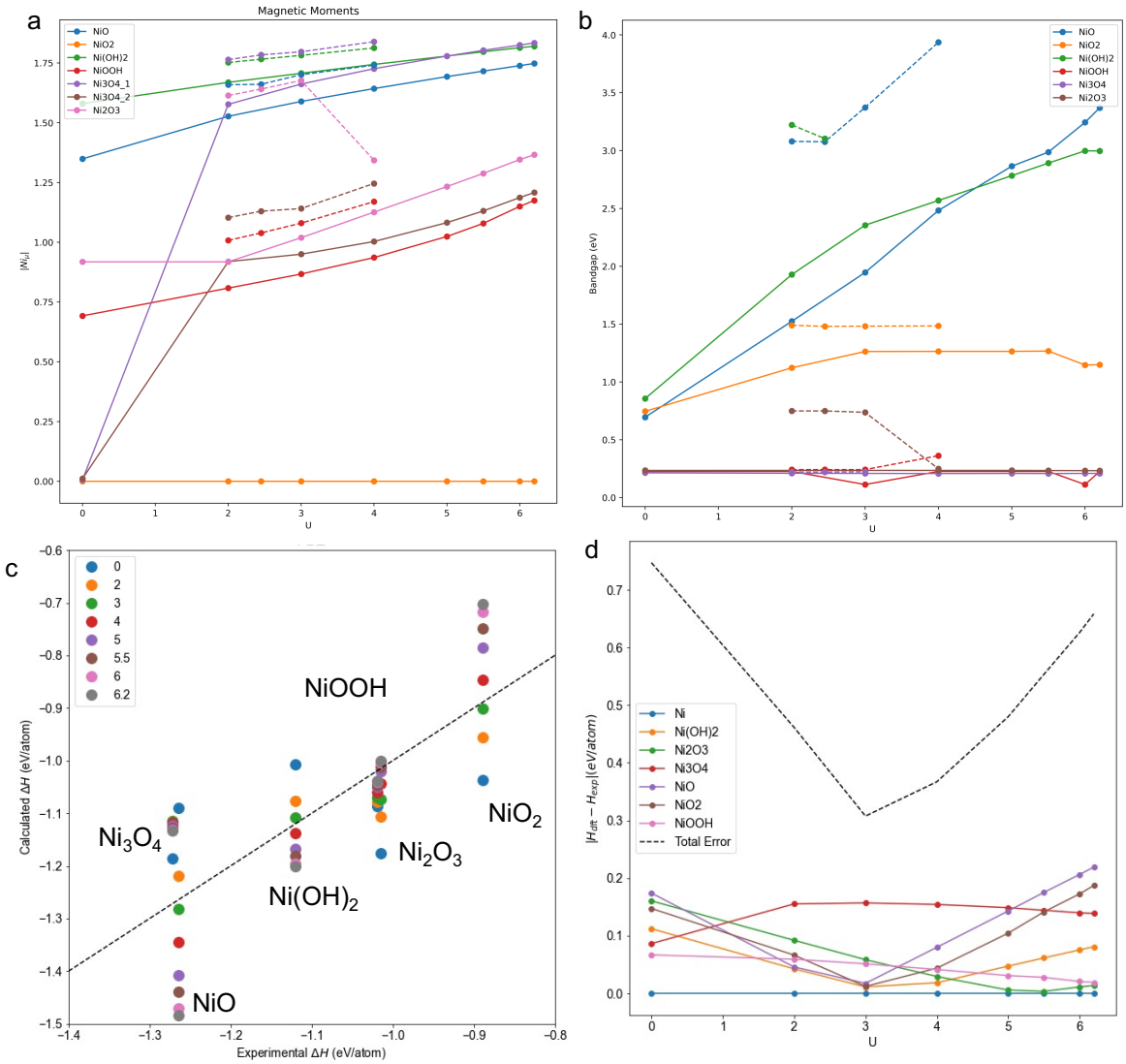

Figure S4: (a) Magnetic moments and (b) bandgap as a function of U value with both SCAN (dashed lines) and PBE functional (solid lines). (c) Enthalpy of formation parity plot against experimental values for NiO_xH_y as a with various U parameters with PBE functional. (d) Error associated with different U parameters for PBE functional

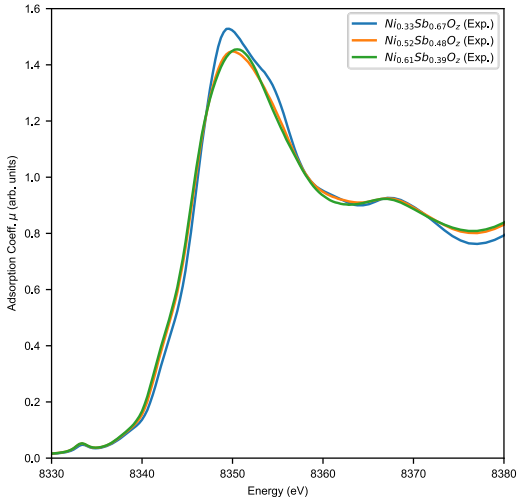

Figure S5: Experimental XAS Ni K-edge for all three samples showing nearly identical peak position.

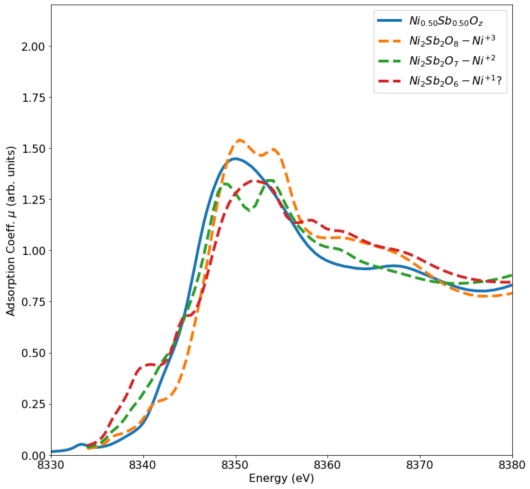

Figure S6: Experimental XAS Ni K-edge for x=0.5 (solid blue line), compared to R-$Ni_4Sb_4O_8$ with 0, 1, and 2 oxygen vacancies in the unit cell

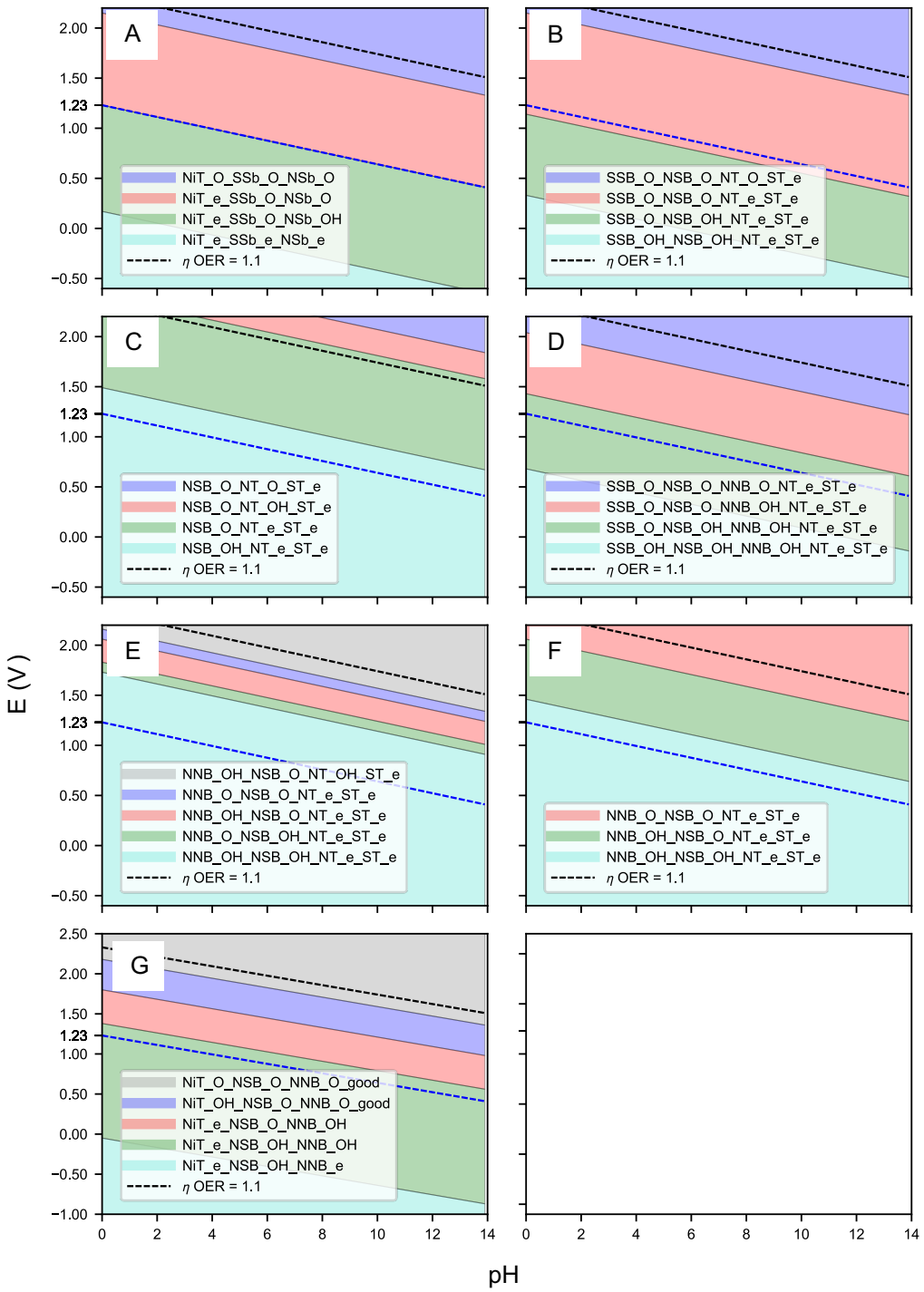

Figure S7: Surface Pourbaix Diagrams for each surface studied in this work. (a, b) R-$Ni_4Sb_2O_{12}$, (c, d) R-$Ni_3Sb_3O_{12}$, (e, f) R-$Ni_4Sb_2O_{12}$, and (g) hex-$Ni_6Sb_3O_{18}$. (a, c, e) show (110) surface terminations, (b, d, f) show (101) surfaces, and (g) is the (100) surface. The specific termination is shown in the legend of each plot where NiT/NT is O_{1c}-N, NSB is O_{2c}-NS, NNB is O_{2c}-NN,

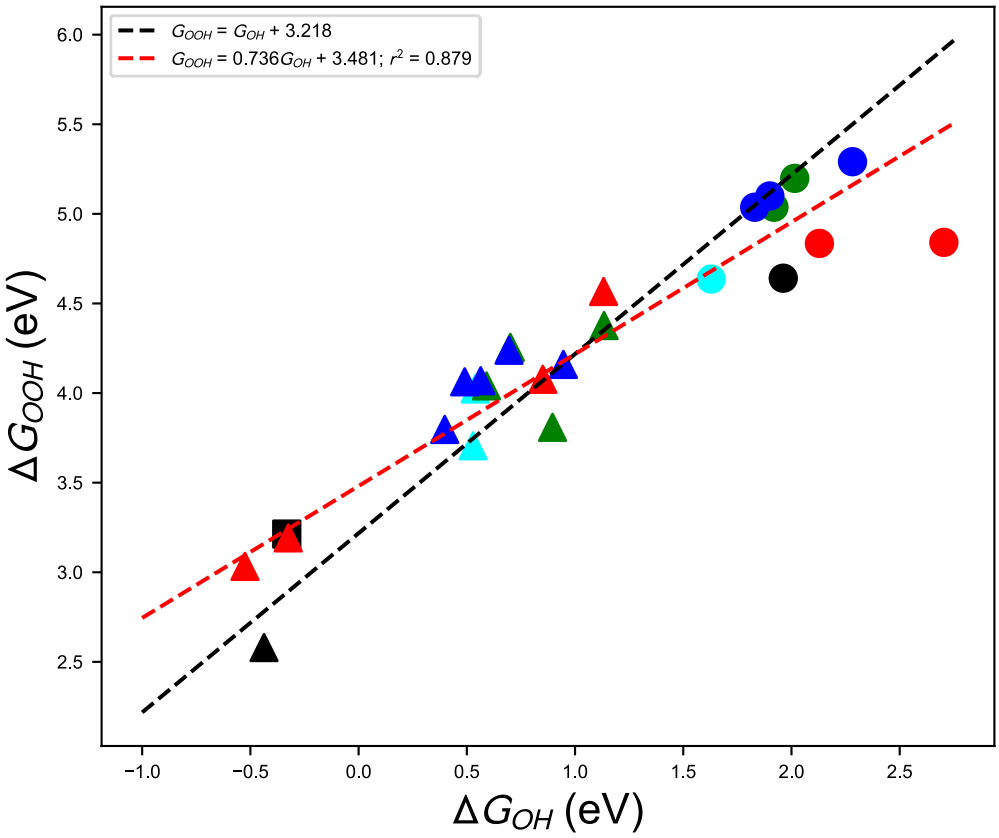

Figure S8: Scaling relationship between ΔG_{*OOH} and ΔG_{*OH} for the Ni-Sb-O systems. Marker symbols and colors have same meanings as in Figure 5a. Ideal scaling show as black dashed line and fitted scaling show as dashed red line.

Table S1: Summary of the bulk ordered structures and compositions used to generate Fig 2. The chemical potentials of O, Sb, and Ni are -5.793, -6.494, and -5.073 eV respectively.

Prototype	Composition	Space Group	Energy (eV/atom)	ΔE_{form} (eV/metal Atom)	ΔE_{hull} (eV/metal atom)
mp-2136	O12 Sb8	Pccn	-118.883	0.323	0.323
mp-230	O16 Sb8	Pna2_1	-144.641	0	0
mp-1705	O20 Sb8	C2/c	-166.28	0.192	0.192
mp-19009	Ni2 O2	Fm-3m	-21.733	0	0
mp-25210	Ni2 O4	C2/m	-31.618	0.85	0.85
P42/mnm	Ni2 O8 Sb2	Pmm2	-67.18	0.575	0.819
P42/mnm	Ni3 O12 Sb3	Cmm2	-103.047	0.195	0.439
P42/mnm	Ni1 O4 Sb1	Cmmm	-34.249	0.245	0.49
P42/mnm	Ni3 O12 Sb3	Cmm2	-103.048	0.195	0.439
P42/mnm	Ni3 O12 Sb3	Cmmm	-102.274	0.324	0.568

P42/mnm	Ni2 O8 Sb2	P-42_1m	-68.886	0.148	0.392
P42/mnm	Ni2 O8 Sb2	Pmma	-68.497	0.245	0.49
P42/mnm	Ni2 O8 Sb2	Pmma	-68.497	0.246	0.49
P42/mnm	Ni2 O8 Sb2	P-42_1m	-68.886	0.148	0.392
P42/mnm	Ni2 O8 Sb2	P-42_1m	-68.695	0.196	0.44
P42/mnm	Ni2 O8 Sb2	P-42_1m	-68.694	0.196	0.441
P63/mmc	Ni2 O8 Sb2	C2/m	-67.411	0.517	0.761
P63/mmc	Ni2 O8 Sb2	C2/c	-65.583	0.974	1.218
P63/mmc	Ni2 O8 Sb2	C2/m	-66.451	0.757	1.001
P63/mmc	Ni1 O4 Sb1	P2/m	-33.776	0.482	0.726
P63/mmc	Ni2 O8 Sb2	P2_1/c	-68.149	0.332	0.577
P42/mnm	Ni2 O8 Sb2	P2	-66.957	0.631	0.875
P42/mnm	Ni2 O8 Sb2	P2_12_12	-66.455	0.756	1
P42/mnm	Ni2 O8 Sb2	P2_12_12	-68.59	0.222	0.467
P42/mnm	Ni1 O4 Sb1	P2/m	-34.265	0.237	0.481
mp-1216649	Ni1 O4 Sb1	Cmmm	-29.738	2.501	2.745
mvc-5693	Ni1 O6 Sb1	Cm	-38.115	4.105	4.35
mp-23018	Ni2 O8 Sb2	C2/c	-66.906	0.643	0.888
mp-1224786	Ni1 O4 Sb1	Cmmm	-29.731	2.504	2.749
mp-674490	Ni2 O8 Sb2	P2/m	-68.169	0.327	0.572
mp-758123	Ni2 O8 Sb2	C2/m	-67.507	0.493	0.737
mvc-5033	Ni2 O12 Sb2	P2_1/c	-80.259	3.098	3.342
mp-1178209	Ni2 O8 Sb2	C222_1	-68.028	0.363	0.607
mp-761281	Ni2 O8 Sb2	Cc	-68.577	0.225	0.47
P42/mnm	Ni2 O12 Sb4	P-42_1m	-105.352	0.048	0.373
P42/mnm	Ni2 O12 Sb4	P-42_1m	-105.432	0.035	0.36
P42/mnm	Ni2 O12 Sb4	Cmmm	-106.3	-0.11	0.216
P42/mnm	Ni2 O12 Sb4	Cmmm	-106.346	-0.118	0.208
P42/mnm	Ni2 O12 Sb4	P4_2/mnm	-107.593	-0.326	0
P42/mnm	Ni2 O12 Sb4	P4_2/mnm	-107.59	-0.325	0.001
P63/mmc	Ni4 O16 Sb8	P2/c	-130.321	2.884	3.21
P63/mmc	Ni4 O16 Sb8	Pbcn	-128.537	3.033	3.359
P63/mmc	Ni4 O16 Sb8	Pbcn	-128.651	3.024	3.349
P63/mmc	Ni2 O8 Sb4	P2_1/c	-64.255	3.035	3.361
P63/mmc	Ni3 O18 Sb6	P321	-160.216	-0.195	0.13
P63/mmc	Ni3 O18 Sb6	P1	-158.213	0.027	0.353
P63/mmc	Ni3 O18 Sb6	P1	-158.234	0.025	0.351
P63/mmc	Ni3 O18 Sb6	C2	-157.2	0.14	0.466
P63/mmc	Ni3 O18 Sb6	P1	-157.682	0.086	0.412
P63/mmc	Ni1 O6 Sb2	P312	-53.015	-0.065	0.261

P63/mmc	Ni3 O18 Sb6	P321	-159.832	-0.153	0.173
P63/mmc	Ni3 O18 Sb6	C2	-157.789	0.074	0.4
mvc-8086	Ni2 O12 Sb4	C2/c	-101.426	0.702	1.028
mvc-1621	Ni2 O12 Sb4	Pmn2_1	-104.37	0.212	0.537
mp-20727	Ni1 O6 Sb2	P-31m	-53.214	-0.131	0.194
mvc-8138	Ni4 O24 Sb8	P2_1/c	-207.715	0.297	0.623
mvc-1659	Ni2 O12 Sb4	Pmn2_1	-104.381	0.21	0.535
mp-25043	Ni6 O36 Sb12	C2	-319.973	-0.17	0.156
mvc-660	Ni2 O16 Sb4	P2/c	-117.551	1.877	2.202
mp-505271	Ni4 O24 Sb8	P4_2/mnm	-215.123	-0.32	0.005
mp-1225944	Ni2 O12 Sb4	P1	-100.332	0.885	1.21
mp-19231	Ni4 O16 Sb8	P4_2/mbc	-162.617	0.193	0.519
mp-754065	Ni1 O6 Sb2	P-31m	-53.192	-0.124	0.202
mvc-8186	Ni4 O24 Sb8	P2_1/c	-207.748	0.294	0.62
mvc-8064	Ni2 O12 Sb4	C2/c	-101.425	0.702	1.028
mp-21908	Ni4 O24 Sb8	P4_2/mnm	-215.135	-0.321	0.004
mp-24845	Ni4 O24 Sb8	P4_2/mnm	-215.135	-0.321	0.004
mp-29892	Ni2 O16 Sb6	P2_1/c	-142.572	-0.097	0.148
mp-1223385	Ni2 O26 Sb10	P2_1/m	-221.404	0.358	0.521
P42/mnm	Ni4 O12 Sb2	P-42_1m	-99.087	0.618	0.781
P42/mnm	Ni4 O12 Sb2	Cmmm	-99.012	0.631	0.794
P42/mnm	Ni4 O12 Sb2	P4_2/mnm	-99.35	0.575	0.737
P42/mnm	Ni4 O12 Sb2	P4_2/mnm	-98.997	0.633	0.796
P42/mnm	Ni4 O12 Sb2	P4_2/mnm	-99.264	0.589	0.752
P42/mnm	Ni4 O12 Sb2	P4_2/mnm	-98.994	0.634	0.797
P42/mnm	Ni4 O12 Sb2	P4_2/mnm	-99.05	0.625	0.787
P42/mnm	Ni4 O12 Sb2	P4_2/mnm	-98.994	0.634	0.797
P63/mmc	Ni6 O18 Sb3	P321	-148.929	0.585	0.748
P63/mmc	Ni6 O18 Sb3	P1	-148.506	0.632	0.795
P63/mmc	Ni6 O18 Sb3	C2	-148.288	0.656	0.819
P63/mmc	Ni6 O18 Sb3	C2	-149.083	0.568	0.731
P63/mmc	Ni12 O36 Sb6	C2	-298.122	0.571	0.733
P63/mmc	Ni12 O36 Sb6	C2	-298.074	0.573	0.736
P63/mmc	Ni2 O6 Sb1	P-31m	-49.475	0.641	0.804
mvc-8086	Ni4 O12 Sb2	C2/c	-96.201	1.099	1.262
mvc-1621	Ni4 O12 Sb2	Pmn2_1	-97.206	0.932	1.095
mp-20727	Ni2 O6 Sb1	P-31m	-49.473	0.642	0.805
mvc-8138	Ni8 O24 Sb4	P-1	-190.961	1.22	1.382
mvc-1659	Ni4 O12 Sb2	Pmn2_1	-97.21	0.931	1.094
mp-25043	Ni12 O36 Sb6	C2	-298.185	0.567	0.73

mvc-660	Ni4 O16 Sb2	P2/c	-111.75	2.37	2.533
mp-505271	Ni8 O24 Sb4	P4_2/mnm	-198.681	0.576	0.739
mp-19231	Ni8 O16 Sb4	P4_2/mbc	-151.647	0.634	0.797
mp-754065	Ni2 O6 Sb1	P-31m	-49.473	0.642	0.805
mp-754065	Ni2 O6 Sb1	P-31m	-49.434	0.655	0.818
mvc-8186	Ni8 O24 Sb4	P2_1	-191.064	1.211	1.374
mvc-8064	Ni4 O12 Sb2	C2/c	-96.194	1.101	1.263
mp-21908	Ni8 O24 Sb4	P4_2/mnm	-198.693	0.575	0.738
mvc-652	Ni4 O16 Sb2	P2/c	-111.719	2.375	2.538
mp-24845	Ni8 O24 Sb4	P4_2/mnm	-198.693	0.575	0.738
mvc-4408	Ni8 O48 Sb12	C2/c	-358.878	1.885	2.178
mvc-4401	Ni8 O48 Sb12	R-3c	-358.974	1.88	2.173
mp-29892	Ni6 O16 Sb2	P2_1/c	-130.048	0.758	0.881
mvc-4408	Ni12 O48 Sb8	R-3c	-346.323	2.229	2.424
mvc-4401	Ni12 O48 Sb8	R-3c	-346.32	2.229	2.424
mvc-8023	Ni6 O24 Sb4	P-1	-173.487	2.196	2.392
mp-754951	Ni4 O12 Sb1	P1	-84.933	2.274	2.372
mp-1223385	Ni10 O26 Sb2	P2_1/m	-192.571	1.814	1.895
mp-757115	Ni10 O26 Sb2	Ama2	-192.286	1.838	1.919

Table S2: Binding energies of OER intermediates for each site on each surface. Same data is plotted in Figure 5.

Bulk Structure	Surface	Site	ΔG_{OH} (eV)	ΔG_{O} (eV)	ΔG_{OOH}-G_{OH} (eV)	Overpotential (V)
NiO2	200	O2c_NN	1.14	1.577	3.017	1.11
NiO2	200	O1c_N	4.176	2.214	2.679	0.984
NiO	111	O3c_N	0.9	1.232	3.545	1.083
hex-Ni2SbO6	100	O1c_N	3.938	2.309	3.007	1.079
hex-Ni2SbO6	100	O2c_NN	2.351	1.822	3.177	0.592
hex-Ni2SbO6	100	O2c_NS	2.31	1.771	3.484	0.541
r-Ni2SbO6	110	O1c_N	4.235	2.22	3.183	0.99
r-Ni2SbO6	110	O2c_NN	2.851	1.717	3.243	0.487
r-Ni2SbO6	110	O2c_NS	2.484	1.893	3.449	0.663
r-Ni2SbO6	101	O1c_N	4.434	2.515	3.118	1.285
r-Ni2SbO6	101	O2c_NN	2.946	2.05	2.913	0.82
r-Ni2SbO6	101	O2c_NS	2.429	1.728	3.554	0.596
r-NiSbO4	110	O1c_N	5.084	2.802	3.009	1.572
r-NiSbO4	110	O2c_NS	2.139	1.741	3.399	0.511
r-NiSbO4	101	O2c_NS1	2.199	1.635	3.505	0.64
r-NiSbO4	101	O2c_NS2	2.093	1.398	3.544	0.916
r-NiSbO4	101	O2c_NN	2.977	2.031	3.214	0.801

r-NiSbO4	101	O2c_SS	1.525	1.035	3.573	1.308
r-NiSbO4	101	O1c_N1	4.322	2.492	3.207	1.262
r-NiSbO4	101	O1c_N2	4.052	2.152	3.2	0.922
r-NiSb2O6	110	O1c_N	4.315	1.611	2.137	1.474
r-NiSb2O6	110	O2c_SS	0.32	0.845	3.558	1.483
r-NiSb2O6	110	O2c_NS	1.159	1.484	3.517	0.803
r-NiSb2O6	101	O1c_N	4.306	2.177	2.706	0.947
r-NiSb2O6	101	O2c_NS	2.25	1.118	3.435	1.087
r-NiSb2O6	101	O2c_SS	1.541	0.69	3.226	1.306

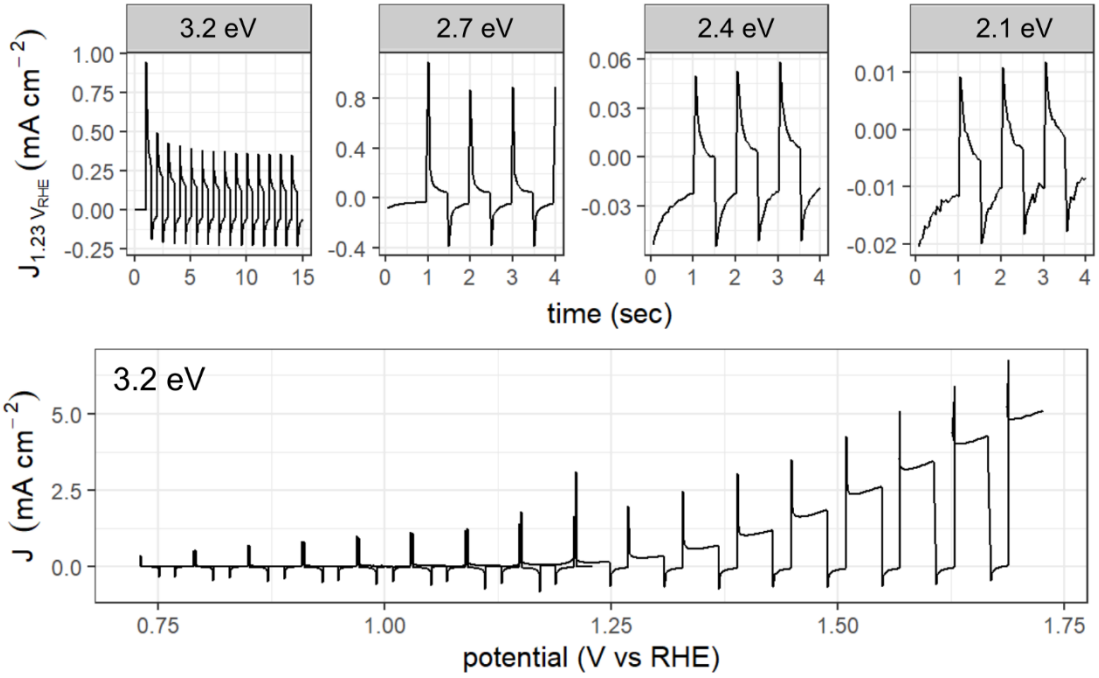

Figure S9: Photoelectrochemical (PEC) characterization of a $Ni_{052}Sb_{0.48}O_z$ film deposited onto SnO_2:F-coated XG glass and annealed at 700 °C. All measurements are in pH 10 borate-buffered electrolyte with 0.1 M sodium sulfite as the sacrificial hole acceptor. The sequence of panels matches that of the experiments, where a series of 4 LEDs from 3.2 to 2.1 eV were used to measure toggled-illumination photoresponse under applied bias of 1.23 V vs RHE. Subsequently, the 3.2 eV LED was used in CV measurement starting at 1.23 V vs RHE with a cathodic sweep followed by an anodic sweep at a rate of 0.02 V s^{-1}. All observed photocurrents are anodic, such that every upward transient in current density corresponds to illumination turn-on and each downward transient corresponds to illumination turn-off.

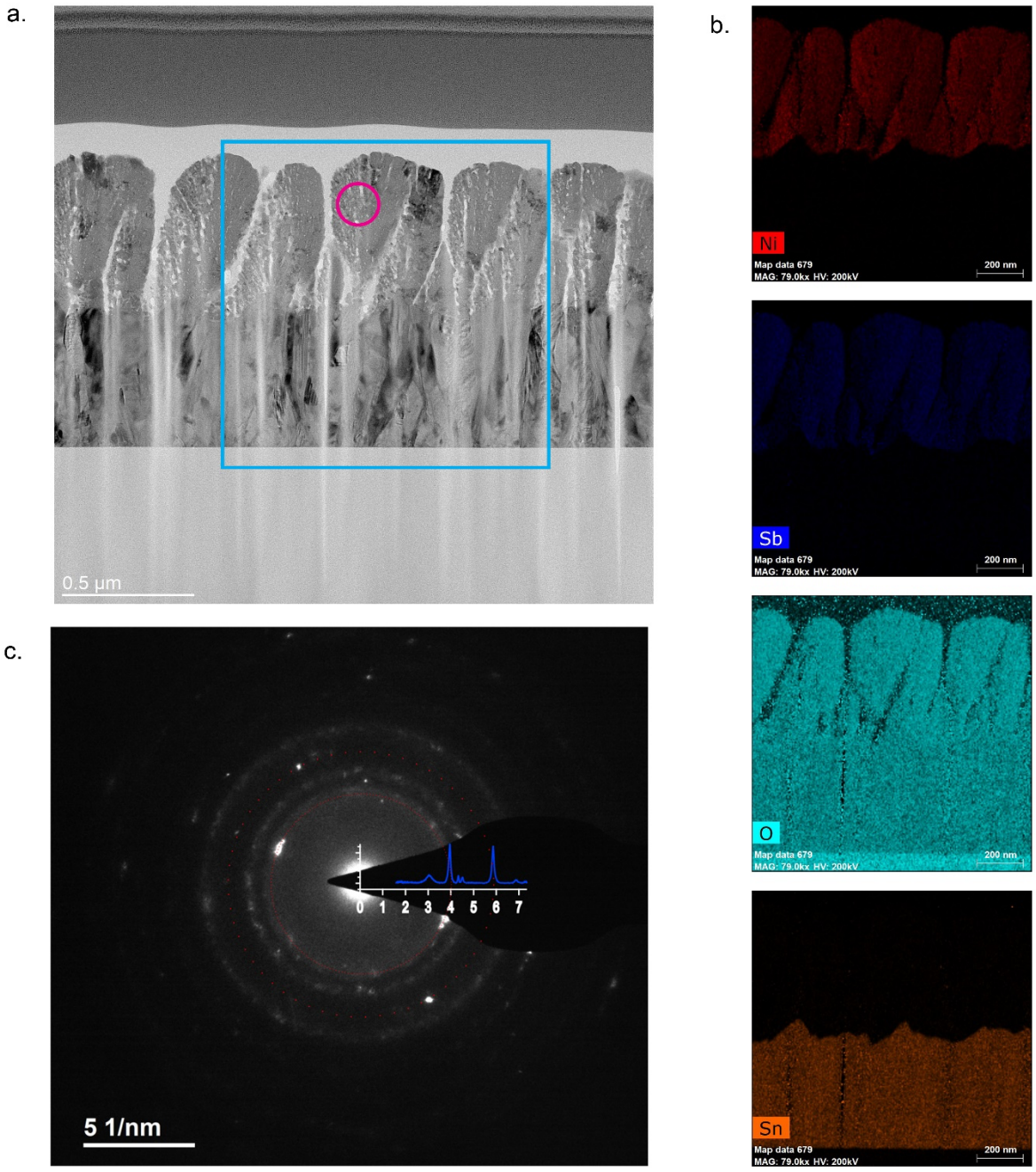

Figure S10: TEM characterization of the $Ni_{052}Sb_{0.48}O_z$ film (deposited on SnO_2:F (FTO)-coated XG glass and annealed at 700 °C) after PEC measurements (see Figure S9) in the pH 10 electrolyte. The cross-section sample was prepared by a focused ion beam. (a) Bright field cross-section TEM image reveals an angled columnar structure that likely arises from the off-axis deposition on the rough FTO coating in the combinatorial synthesis. Hall measurements on a duplicate film indicate a high resistance, which is likely due to the lack of lateral conduction from the presence of voids in between column grains. The electrochemical results of Figure 5 indicate that electronic conduction does not interfere with characterization of catalytic activity. (b) Individual color maps for the four elements of interest: Ni, Sb, O, and Sn, obtained by energy dispersive x-ray

spectroscopy (EDX) in the region indicated by cyan square in (a). These maps confirm that there is no detectable interdiffusion of Sn from the conducting support and Ni/Sb from the deposited film. (c) The selected area electron diffraction (SAED) image taken from the area indicated by magenta circle in (a), along with the XRD pattern of the $Ni_{049}Sb_{0.51}O_z$ film (deposited on SiO_2/Si and annealed at 700 °C) plotted as a function of scattering vector, 1/d, in nm^{-1}, where d is the lattice plane spacing. This XRD pattern is the same data shown in Figure 1b blue curve, where it is plotted as a function of diffraction angle, 2θ, in degrees. In addition to the absence of the strongest rutile (110) peak, the two major diffraction peaks (101) and (211) around 3.95 and 5.83 nm^{-1}, respectively, match well with the bright diffraction spots in the SAED image. The agreement of diffraction patterns confirms the two thin films grown on FTO and SiO_2/Si have the same crystalline structure, which is disordered rutile structure with space group Pnnm as theory predicted in Figure 1.